Joint FWI for velocity model building: a real case study in the viscoacoustic approximation

W. Zhou[*†], *R. Brossier*[†], *S. Operto*[‡], *J. Virieux*[†], *P. Yang*[†]
[†] *ISTerre, Univ. Grenoble Alpes,* [‡] *Géoazur-CNRS, Univ. Nice–Sophia-Antipolis*

SUMMARY

Joint full waveform inversion (JFWI) combines reflection (RWI) and early-arrival (EWI) waveform inversions to build a large-scale velocity model of the subsurface. It is alternated with a waveform inversion/migration of near-offset reflections to build a short-scale impedance model that is used as an input to build the sensitivity kernel of RWI along the two-way reflection paths. The velocity macromodel built by JFWI can be used as the initial model of standard FWI to enrich the high wavenumber content of the model. We present an application of this workflow to a real 2D OBC profile across a gas cloud in the North Sea. First, we highlight the footprint of attenuation by comparing recorded seismograms with the synthetics computed in a viscoacoustic velocity model previously developed by 3D FWI. Then, the main promises and pitfalls of JFWI are highlighted using two initial models of increasing accuracy. When starting from a crude 1D initial model, JFWI is influenced by cycle-skipping artifacts and fails to update the low-wavenumber content of the subsurface model. When a more accurate initial model is used, the procedure of JFWI followed by standard FWI (with resulting JFWI model as initial model) succeeds in building a velocity model which is more accurate than the one built directly by standard FWI. This study suggests that JFWI is more efficient than FWI to update the low horizontal wavenumbers along the reflection wavepaths during the velocity macromodel building task, hence leading to a more accurate reconstruction of the gas cloud. However, it remains prone to cycle skipping when a conventional difference-based misfit function is considered. Therefore, more robust misfit function must be used in the future to reduce the demand on an accurate initial model.

INTRODUCTION

With the development of long-offset wide-azimuth acquisition geometries, waveform inversion of early arrivals (EWI) such as diving waves and wide-angle reflections is useful to build an accurate velocity model (Virieux and Operto, 2009). However, the limitation of EWI is the insufficient sensitivity to deep structures that are below the maximum penetration depth of early arrivals. In addition, a brute-force application of EWI is often prevented by cycle skipping issue due to long propagation distances when very low frequencies are unavailable (e.g. Warner and Guasch, 2014; Luo et al., 2016; Métivier et al., 2016). Alternatively, reflection waveform inversion (RWI) (e.g. Xu et al., 2012; Wang et al., 2013; Brossier et al., 2015) has been proposed to build the velocity model by restricting the sensitivity kernel of full waveform inversion (FWI) along the two-way transmission paths of short-spread reflections, hence increasing the depth sensitivity compared to EWI. A short-scale reflectivity model, produced by migration/inversion of reflection data, is used as an input to build the RWI gradient. A key property of RWI is the significant reduction of cycle-skipping issues in short offset ranges.

Due to the different wavepaths involved in EWI and RWI, the two inversion schemes tend to preferentially sample the vertical and horizontal wavenumber components of the velocity model, respectively. This prompts us to combine EWI and RWI into a joint inversion (JFWI) to broaden the wavenumber spectrum of the velocity model (Zhou et al., 2015). They show with a synthetic experiment that JFWI outperforms RWI for near-surface reconstruction, which translates to more accurate reflector images at great depths. A real-case study further reveals that JFWI is still sensitive to cycle skipping mainly caused by early arrivals, which leads us to implement a layer-stripping approach by offset continuation (Zhou et al., 2016). However, we did not account for attenuation, the footprint of which in the wavefield is not negligible in this target zone (Prieux et al., 2011; Operto et al., 2015).

The sensitivity of FWI to attenuation effects has been reviewed in Kurzmann et al. (2013), who have shown a significant improvement of the velocity model when attenuation is accounted for during seismic modeling, even in an approximate way. Therefore, we are motivated to re-assess JFWI when seismic modeling is performed with attenuation. In this abstract, we shall first illustrate the attenuation footprint in the data set, and then assess the sensitivity of JFWI to cycle skipping issues. The velocity macromodel built by JFWI will be further assessed in terms of kinematic accuracy and spatial resolution as an initial model for FWI.

METHODOLOGY

Two key ingredients of JFWI are, on the data side, the explicit separation between the early arrivals d^e and short-spread reflections d^r and on the model side, the scale separation between the velocity macromodel V_P and the short-scale impedance model I_P (Jannane et al., 1989; Operto et al., 2013). The weighted misfit function of JFWI writes (Zhou et al., 2015)

$$C(V_P)|_{I_P} = \frac{1}{2}\|W^e\left(d^e - Ru_0\right)\|^2 + \frac{1}{2}\|W^r\left(d^r - R\delta u\right)\|^2,$$

where the background wavefield u_0 is computed in the smooth V_P model. The full scattered wavefield δu is the difference between the full wavefield u that is computed in the smooth V_P and rough I_P models and the background wavefield (i.e. $\delta u = u - u_0$). The explicit data separation between early arrivals and reflections is needed to evaluate the two corresponding independent L_2 functionals, the gradient of which naturally excludes the high-wavenumber migration isochrones (first order). Such separation may require a careful preprocessing as reviewed in Zhou et al. (2015). The computational cost of the JFWI is twice of standard FWI while no memory overhead is required. The overall workflow consists of the following steps starting from smooth V_P and I_P models (Zhou et al., 2015): [1] Least-squares migration of near-offset reflections to generate I_P perturbations; [2] JFWI to update smooth V_P; [3] Go back to

Step [1] until convergence. The repetition of Step [1] is needed to recreate I_P perturbations consistently with new V_P models while keeping the background component of I_P fixed to its initial value, such that near-offset reflections are still matched during Step [2].

DATA ANATOMY: TOWARDS VISCOACOUSTIC MODELING

We apply JFWI to an OBC line acquired in the North Sea. A velocity model has been built by 3D reflection traveltime tomography (Fig. 1a), which shows a low-velocity gas area (blue area) embedded in the soft sediments above the caprock at 2.4 km depth (Barkved et al., 2010; Haller et al., 2016). Using the tomographic model as the initial model, various applications of 3D FWI (e.g., Sirgue et al., 2010; Operto et al., 2015) have largely increased the resolution of the subsurface models (Fig. 1b).

Two frequency bands, 3–5.1 Hz and 3–7.1 Hz, are sequentially considered for inversion (Bunks et al., 1995). Gibbs effect after band-pass filtering was mitigated by reshaping the source wavelets estimated from zero offset traces. The main phases identified in Fig. 2a are direct and diving waves (yellow arrows), short-spread reflections from shallow reflectors (blue) and the sediment-caprock interface (red). At far offsets, the postcritical reflections (dashed red) and refractions (dashed magenta) from the sediment-caprock interface provide low-wavenumber sensitivity down to 2.5 km depth and are treated as early arrivals accordingly. Based on this phase identification, we define the offset-dependent time window function for data separation as shown in Fig. 2a, yellow line.

Before inversion, we cautiously made a decision concerning the modeling tool for wavefield simulation. Faithful anisotropic models (ε and δ) are available (courtesy of BP) and the elastic footprint in the data set can be neglected (Operto et al., 2015, their figure 23). However, this VTI acoustic approximation of wave propagation is not kinematically accurate enough as suggested by the non-negligible mismatches in Fig. 2b, black arrow, between the recorded diving waves and the synthetics that are computed in the existing 3D FWI velocity model of Operto et al. (2015). We attribute these mismatches to attenuation caused by the gas cloud and soft sediments.

To account for attenuation effects, we use three standard linear solid (SLS) mechanisms (Emmerich and Korn, 1987; Carcione et al., 1988; Robertsson et al., 1994; Moczo and Kristek, 2005) to achieve a nearly frequency-independent Q_P (Plessix, 2016; Yang et al., 2016). For simplicity, we assume $Q_P = 1000$ in the water layer, $Q_P = 95.17 \times (V_P - 1.3)^{2.5} + 50$ for $1.5 \leq V_P \leq 2.5$ km/s giving $Q_P \approx 60$ in the gas cloud, and $Q_P = 200$ below the caprock (Fig. 1c,d). As expected, this viscoacoustic modeling engine allows for an improved data fit, especially for the direct wave and postcritical reflection (Fig. 2c). Although a better fit of diving waves and postcritical reflections is achieved with 3D modeling (Fig. 2d), we limit our study to 2D geometry for sake of numerical efficiency. The 2D assumption raises the issue of the footprint of the out-of-plane effects. Nevertheless, we shall leave them in the data set and processed them during inversion as coherent noise.

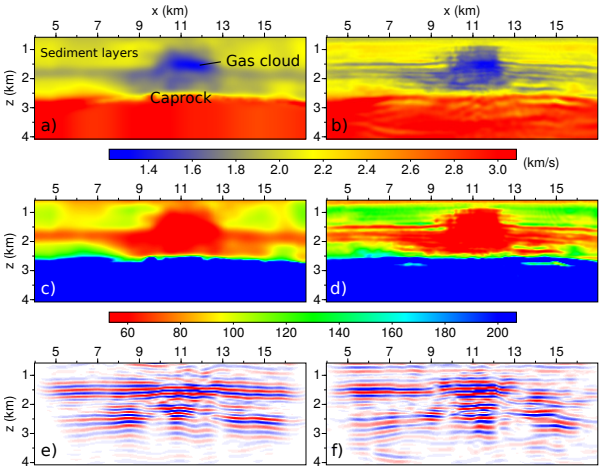

Figure 1: 2D sections of V_P models built by (a) reflection tomography (Courtesy of BP) and (b) 3D FWI (Operto et al., 2015). Corresponding Q_P models (c,d) and migrated images (e,f) inferred from (a,b), respectively.

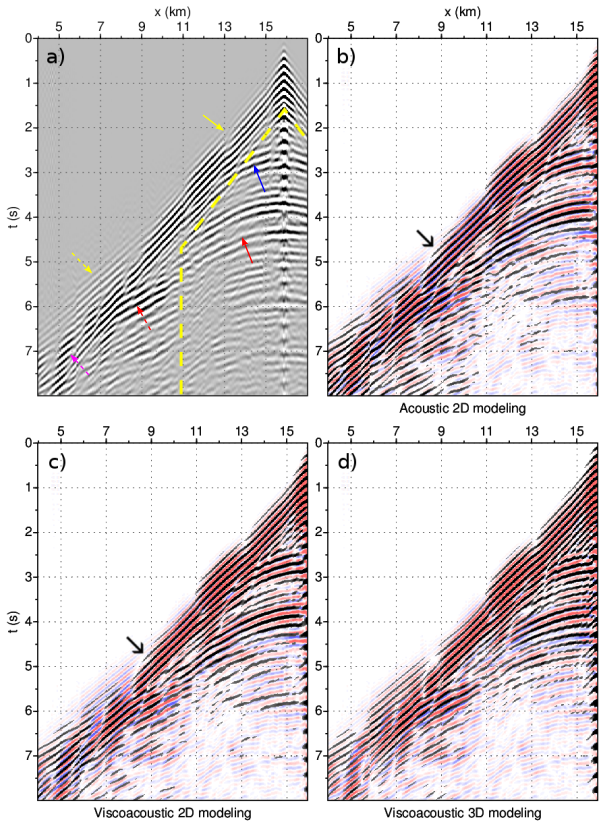

Figure 2: (a) One receiver gather of real data after low-pass filtering (cutoff at 7.1 Hz) and wavelet reshaping. (b-d) Same gather plotted in a blue-white-red color scale. The overlaid synthetics (black wiggles) are computed in the V_P model of Fig. 1b with different modeling engines (titled below). The two data sets are in phase if the black wiggles cover the blue area. An increasing level of data fit is observed from (b) to (d) (black arrows). To achieve potentially acceptable data fit while avoiding cumbersome computations, we use viscoacoustic 2D modeling in this study.

RESULTS

Joint FWI

We shall use two initial models of increasing accuracy to test the sensitivity of JFWI to the initial model. The first one is built by smoothing the tomographic model below the see bed to remove the reflectivity component followed by a lateral averaging (Fig. 3a). Hence, the purpose of using this 1D model is to assess whether JFWI can recover the lateral variations generated by the gas cloud. We assess the velocity model by computing migrated images or I_P perturbations by IpWI. The flatness of the sediment-caprock interface, revealed by former studies, is used to assess the faithfulness of the velocity in the gas cloud (Fig. 1e,f). The migrated image computed in the 1D initial model shows the deepening of the sediment-caprock interface below the gas cloud (Fig. 3c), which results from overestimated velocities in the overburden.

Fig. 3b shows the inversion result. Not having imaged the gas cloud, JFWI creates a pair of high-velocity anomalies along reflection paths above the caprock together with a low-velocity blob in the middle of the gas cloud. This velocity artifacts in the overburden leads to an inaccurate migrated image highlighted by the non-flatness of the caprock reflector (Fig. 3d).

Fig. 3c,d shows the data fit achieved by the 1D initial and the resulting JFWI V_P models, in which the I_P perturbations are added to generate reflected waves. Both V_P models provide good data match at short offsets. The postcritical reflections are missing in the synthetic data; these phases may either not be produced or interfere with diving/refracted waves, due to the high velocities in the overburden, and hence are not observable. On the other hand, an improved fit of refractions is shown after JFWI; however, this is a cycle-skipped fit. To verify this statement, we show the seismograms at the $x = 5$ km position in Fig. 4. It is obvious that JFWI has decreased the least-squares based misfit function at the price of a larger traveltime lag, leading to the aforementioned high-velocity artifacts (Fig. 3b).

We build a second initial model by smoothing the tomographic model such that the the large-scale trend of the gas cloud is preserved (Fig. 5a). Unlike the 1D initial model, this 2D initial model generates migrated image with a flat cap-rock reflector (Fig. 5c) as the smoothing, less aggressive than averaging, does not significantly degrade the kinematic accuracy of the original tomographic model.

Fig. 5b shows the JFWI result. No cycle skipping is witnessed. Sufficiently low velocities are recovered in the gas cloud preserving flat structures in the migrated image (Fig. 5d). To further assess this JFWI model as an initial model for FWI, we perform standard FWI with a classical frequency continuation scheme that inverts the 5.1 Hz data set before the 7.1 Hz one. The final FWI model shows a reasonable broadband reconstruction of the subsurface (Fig. 5e).

The low-velocity blob in the 2D initial model improves the fit of the postcritical reflections (Fig. 6a) compared with the 1D initial model (Fig. 3e). However, some mismatches are still visible, implying a deficit of low wavenumbers in this model. Fig. 6b,c show the data fit for the 5.1 Hz JFWI model and

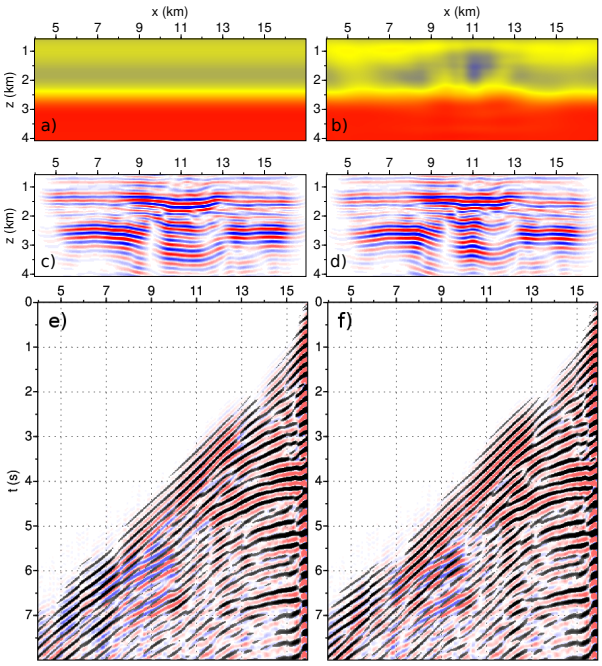

Figure 3: (a) 1D initial model. (b) Final JFWI velocity model. (c,d) Corresponding migrated images. (e,f) Data fit at 5.1 Hz. Note the synclinal-shape caprock image resulting from overestimated velocities in the overburden.

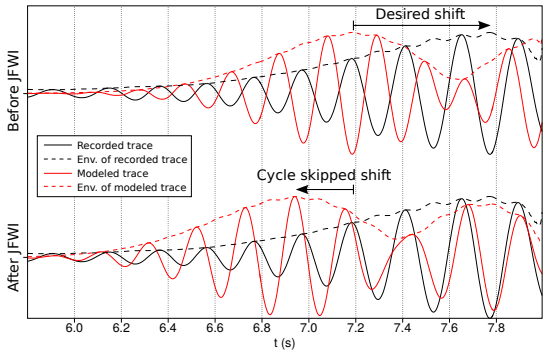

Figure 4: Cycle skipping. Zoom of the refracted wave at $x = 5$ km (Figs 3e,f). The waveform envelopes (dash lines) help quantify the traveltime which is undesirably increased after inversion.

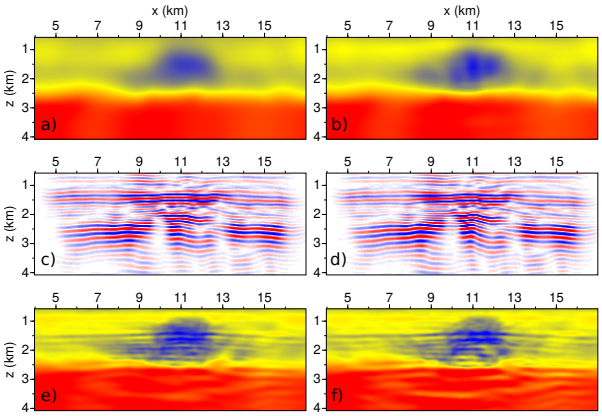

Figure 5: (a) 2D initial model. (b) Final JFWI velocity model. (c,d) Corresponding migrated images. (e) FWI velocity model starting from (b). (f) FWI velocity model starting from (a).

7.1 Hz subsequent FWI model, respectively. The former shows an improved data fit suggesting a reliable update of the large-scale velocity variations by JFWI. The latter also shows a good fit expect for the postcritical reflections at $x = 7$ km position (Fig. 6c, black arrow), which is a desirable mismatch as these reflections come from out-of-plane propagation. We admit that we have a pity cycle-skipping phenomenon for near-offset direct waves at the border of the near-surface (gray arrow). A 3D inversion combined with more prudent frequency continuation schemes may help solve this problem (Operto et al., 2015).

Standard FWI

To assess the effectiveness of JFWI in initial macro model building for FWI, we perform FWI using the 2D smooth model (Fig. 5a) as initial model. The result is shown in Fig. 5f. We also show in Fig. 7 the direct comparison between the two FWI results along an horizontal profile at 2.3 km depth crossing the gas cloud. Both suggest that the FWI result starting from the JFWI model has a higher lateral resolution in the gas cloud with a richer low wavenumber content than the other FWI result. This is because JFWI has succeeded to update the low horizontal wavenumbers along sub-vertical wavepaths connecting the reflectors to the surface, whereas FWI is more suitable to update the low vertical wavenumbers along the wavepaths associated with wide-aperture arrivals (diving waves and postcritical reflections).

Such deficit of low wavenumbers in the FWI model of Fig. 5f cannot be easily detected when we assess the accuracy of the model through data fit (Fig. 6d). The improved match of diving wave by the standard FWI model is undesirable as these waves have underwent out-of-plane propagation. In order to reduce the misfit function, standard FWI may have shifted the synthetic postcritical reflections to earlier traveltimes, leading to overestimated velocities in the gas cloud as shown in Fig. 7, black arrow. In contrast, it seems that the higher sensitivity of JWI to lateral subsurface variations has prevented such artifacts and helped recover the low velocities in the gas cloud although the misfit value is slightly higher.

CONCLUSIONS

We have combined the sensitivity kernels associated to early arrivals and reflections for velocity macromodel building that is suitable for standard FWI implementation. The approach has been applied to a 2D OBC data set collected across a gas cloud. We have considered attenuation in the wave simulation part of the inversion, the significance of which has been illustrated on the postcritical reflections and refracted waves from below the gas cloud (i.e. early arrivals at far offsets). However, the associated cycle-skipping issue has prevented us from using a crude initial model. Therefore, it is still required to design a decent initial model for the proposed least-squares based misfit function. When using this initial model, the workflow that alternates JFWI and impedance waveform inversion builds an enough accurate initial model for standard FWI: low velocities are nicely reconstructed in the gas cloud, unlike the direct application of FWI considering the same initial model that we have taken for JFWI. Further investigations should deal with alternative misfit function to mitigate cycle skipping as well as extensions to 3D geometry to take advantage of broader aperture illumination and account more accurately for 3D wave propagation effects.

Acknowledgements This study was funded by the SEISCOPE consortium, sponsored by CGG, CHEVRON, EXXON-MOBIL, JGI, SHELL, SINOPEC, STATOIL, TOTAL and WOODSIDE. This study was granted access to the HPC resources of CIMENT infrastructure and CINES/IDRIS under the allocation 046091 made by GENCI. The authors thank BP Norge AS and Hess Norge AS for providing the data set and the permission to publish this work. The first author appreciates fruitful discussions with F. Audebert (TOTAL), H. Chauris (MinesParisTech), A. Górszczyk (PAN), G. Lambaré (CGG), L. Métivier (LJK-CNRS, UGA), and R.-E. Plessix (Shell).

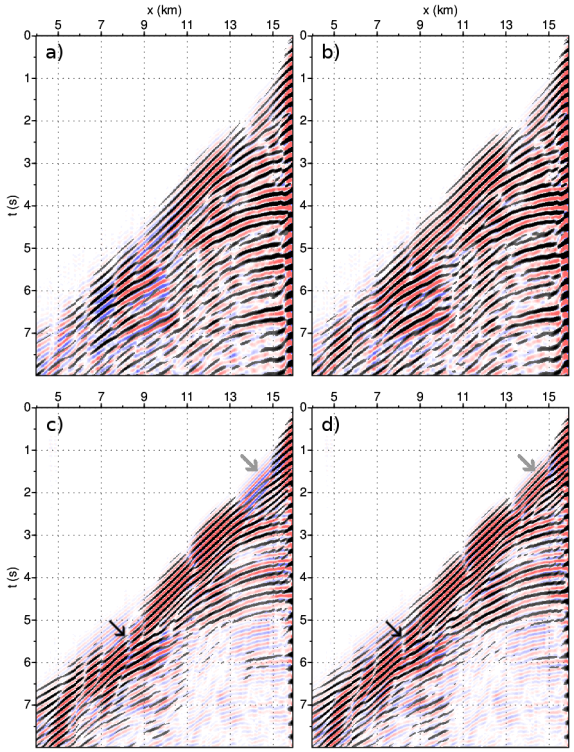

Figure 6: Data fit at 5.1 Hz (a,b) and 7.1 Hz (c,d). Synthetics are computed in (a) 2D initial model (Fig. 5a), (b) JFWI model (Fig. 5b), (c) FWI result using JFWI model (Fig. 5e), and (d) FWI result using 2D initial model (Fig. 5f). Compared with (c), the FWI data fit of (d) shows a over-fitting of the postcritical reflections (black arrows) despite a better match of shallow transmitted waves (gray arrows).

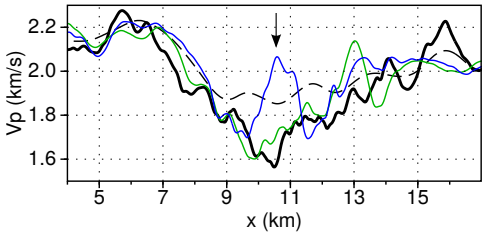

Figure 7: Horizontal profiles at 2.3 km depth of the 3D FWI model (Fig. 1b) (black) as reference, 2D smooth model (dashed), FWI result using JFWI model (green) and FWI result using 2D initial model (blue). Note the deviation of the former FWI model resulting from the over-fitting of the postcritical reflections (black arrow), whereas JFWI followed by FWI matches reasonably well the reference profile.

EDITED REFERENCES

Note: This reference list is a copyedited version of the reference list submitted by the author. Reference lists for the 2017 SEG Technical Program Expanded Abstracts have been copyedited so that references provided with the online metadata for each paper will achieve a high degree of linking to cited sources that appear on the Web.

REFERENCES

Barkved, O., U. Albertin, P. Heavey, J. Kommedal, J. van Gestel, R. Synnove, H. Pettersen, and C. Kent, 2010, Business impact of full waveform inversion at Valhall: 91st SEG Annual International Meeting, https://doi.org/10.1190/1.3513929.

Brossier, R., S. Operto, and J. Virieux, 2015, Velocity model building from seismic reflection data by full waveform inversion: Geophysical Prospecting, **63**, 354–367, https://doi.org/10.1111/1365-2478.12190.

Bunks, C., F. M. Salek, S. Zaleski, and G. Chavent, 1995, Multiscale seismic waveform inversion: Geophysics, **60,** no. 5, 1457–1473, https://doi.org/10.1190/1.1443880.

Carcione, J., D. Kosloff, and R. Kosloff, 1988, Wave propagation simulation in a linear viscoacoustic medium: Geophysical Journal International, **93**, 393–401, https://doi.org/10.1111/j.1365-246x.1988.tb02010.x.

Emmerich, H., and M. Korn, 1987, Incorporation of attenuation into time-domain computation of seismic wavefield: Geophysics, **52**, 1252–1264, https://doi.org/10.1190/1.1442386.

Haller, N., R. Flateboe, C. Twallin, V. Dahl-Eriksen, P. Heavey, E. Kjos, R. Milne, and W. Rietveld, 2016, Valhall case study — value of seismic technology for reducing risks in a reactive overburden: Presented at the 78th EAGE Annual Meeting, https://doi.org/10.3997/2214-4609.201600817.

Jannane, M., W. Beydoun, E. Crase, D. Cao, Z. Koren, E. Landa, M. Mendes, A. Pica, M. Noble, G. Roeth, S. Singh, R. Snieder, A. Tarantola, and D. Trezeguet, 1989, Wavelengths of Earth structures that can be resolved from seismic reflection data: Geophysics, **54**, 906–910, https://doi.org/10.1190/1.1442719.

Kurzmann, A., A. Przebindowska, D. Kohn, and T. Bohlen, 2013, Acoustic full waveform tomography in the presence of attenuation: a sensitivity analysis: Geophysical Journal International, **195**, 985–1000, https://doi.org/10.1093/gji/ggt305.

Luo, Y., Y. Ma, Y. Wu, H. Liu, and L. Cao, 2016, Full-traveltime inversion: Geophysics, **81**, R261–R274, https://doi.org/10.1190/geo2015-0353.1.

Metivier, L., R. Brossier, Q. Merigot, E. Oudet, and J. Virieux, 2016, Measuring the misfit between seismograms using an optimal transport distance: Application to full waveform inversion: Geophysical Journal International, **205**, 345–377, https://doi.org/10.1093/gji/ggw014.

Moczo, P., and J. Kristek, 2005, On the rheological models used for time-domain methods of seismic wave propagation: Geophysical Research Letters, **32**, https://doi.org/10.1029/2004gl021598.

Operto, S., R. Brossier, Y. Gholami, L. Metivier, V. Prieux, A. Ribodetti, and J. Virieux, 2013, A guided tour of multiparameter full waveform inversion for multicomponent data: from theory to practice: The Leading Edge, **32**, 1040–1054, https://doi.org/10.1190/tle32091040.1.

Operto, S., A. Miniussi, R. Brossier, L. Combe, L. Metivier, V. Monteiller, A. Ribodetti, and J. Virieux, 2015, Efficient 3-D frequency-domain mono-parameter full-waveform inversion of ocean-bottom cable data: application to Valhall in the visco-acoustic vertical transverse isotropic approximation: Geophysical Journal International, **202**, 1362–1391, https://doi.org/10.1093/gji/ggv226.

Plessix, R., 2016, Visco-acoustic full waveform inversion: Presented at the 78th EAGE Annual Meeting, https://doi.org/10.3997/2214-4609.201600827.

Prieux, V., R. Brossier, Y. Gholami, S. Operto, J. Virieux, O. Barkved, and J. Kommedal, 2011, On the footprint of anisotropy on isotropic full waveform inversion: the Valhall case study: Geophysical Journal International, 187, 1495–1515, https://doi.org/10.1111/j.1365-246x.2011.05209.x.

Robertsson, J., J. Blanch, and W. Symes, 1994, Viscoelastic finite-difference modeling: Geophysics, **59**, 1444–1456, https://doi.org/10.1190/1.1443701.

Sirgue, L., O. I. Barkved, J. Dellinger, J. Etgen, U. Albertin, and J. H. Kommedal, 2010, Full waveform inversion: the next leap forward in imaging at Valhall: First Break, **28**, 65–70.

Virieux, J., and S. Operto, 2009, An overview of full waveform inversion in exploration geophysics: Geophysics, 74, WCC1-WCC26.

Wang, S., F. Chen, H. Zhang, and Y. Shen, 2013, Reflection-based full waveform inversion (RFWI) in the frequency domain: SEG Technical Program Expanded Abstracts, SEG, 877–881, https://doi.org/10.1190/segam2013-0671.1.

Warner, M., and L. Guasch, 2014, Adaptative waveform inversion — FWI without cycle skipping — theory: 76th EAGE Conference and Exhibition 2014, We E106 13.

Xu, S., D. Wang, F. Chen, G. Lambare, and Y. Zhang, 2012, Inversion on reflected seismic wave: SEG Technical Program Expanded Abstracts 2012, 1–7, https://doi.org/10.1190/segam2012-1473.1.

Yang, P., R. Brossier, L. Metivier, and J. Virieux, 2016, A review on the systematic formulation of 3D multiparameter full waveform inversion in viscoelastic medium: Geophysical Journal International, 207, 129–149, https://doi.org/10.1093/gji/ggw262.

Zhou, W., R. Brossier, S. Operto, and J. Virieux, 2015, Full waveform inversion of diving and reflected waves for velocity model building with impedance inversion based on scale separation: Geophysical Journal International, 202, 1535–1554, https://doi.org/10.1093/gji/ggv228.

Zhou, W., R. Brossier, S. Operto, and J. Virieux, 2016, Joint full waveform inversion of early arrivals and reflections: A real obc case study with gas cloud: SEG Technical Program Expanded Abstracts 2016, SEG, 1247–1251, https://doi.org/10.1190/segam2016-13954099.1.